

## Chapter IV

### Estimates of the Rate Coefficients for Chain Initiation, Propagation, and Termination during Fischer-Tropsch Synthesis over Ru/TiO<sub>2</sub>

#### ABSTRACT

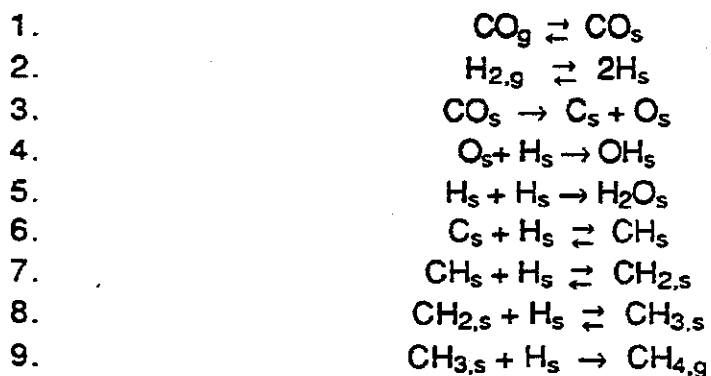
Transient response isotopic tracer experiments have been used to study chain growth during Fischer-Tropsch synthesis over a Ru/TiO<sub>2</sub> catalyst. This involves observation of the incorporation of <sup>13</sup>C into reaction products after an abrupt switch from <sup>12</sup>CO/D<sub>2</sub> to <sup>13</sup>CO/D<sub>2</sub> in the feed. Values for the rate constants for initiation, propagation and termination are determined by fitting theoretically generated model curves to the observed transient responses. The rate constant for chain initiation is independent of temperature and D<sub>2</sub>/CO ratio. The rate constants for propagation and termination increase with temperature. The rate constant for propagation is not affected by the D<sub>2</sub>/CO ratio. The rate constant for termination increases linearly with increasing D<sub>2</sub>/CO ratio. The activation energy for chain termination is significantly higher than that for chain propagation, explaining the observed decrease in chain growth probability,  $\alpha$ , with increasing temperature. Coverages by reaction intermediates are also estimated. The dominant species are monomeric building units which occupy 0.2-0.6 ML. Alkyl species

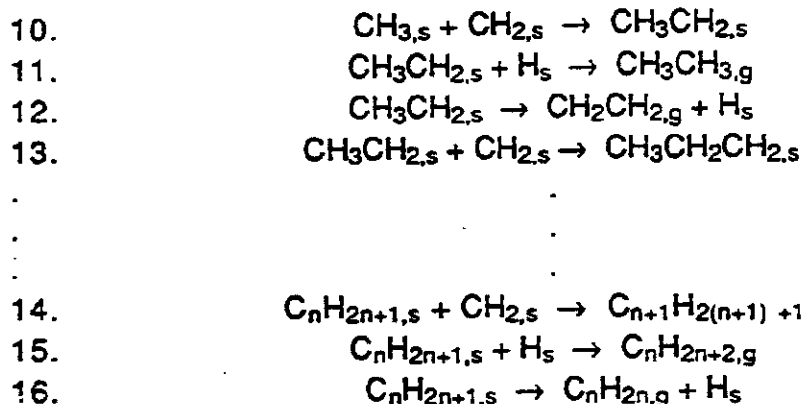
that are the direct hydrocarbon product precursors occupy < 0.2 ML  
and adsorbed CO covers 0.7 ML.

## 1.0 INTRODUCTION

Fischer-Tropsch synthesis (FTS) produces a spectrum of products consisting primarily of linear olefins and alkanes (1). The carbon number distribution of the products containing four or more carbon atoms is often well described by an Anderson-Schulz-Flory (ASF) distribution, which assumes that products containing  $n$  carbon atoms are produced by a stepwise polymerization of  $C_1$  species (2). If the probability of chain growth,  $\alpha$ , defined as the ratio of the rate of chain propagation to the sum of the rates of chain propagation and termination, is taken to be independent of  $n$ , then  $[N_{C_{n+1}}]/[N_{C_n}] = \alpha$ , where  $N_{C_n}$  and  $N_{C_{n-1}}$  are the turnover frequencies for products containing  $n$  and  $n+1$  carbon atoms, respectively. Steady state investigations of FTS have shown that  $\alpha$  is a complex function of both temperature and the partial pressures of  $H_2$  and  $CO$  (2-5).

Mechanistic studies of hydrocarbon production by FTS over Fe, Co and Ru suggest that the mechanism of FTS might be described by the following reaction sequence (6):





Adsorbed CO covers most of the catalyst surface and is in equilibrium with gas-phase CO (6-8). Likewise, dissociatively adsorbed H<sub>2</sub> is found to be in equilibrium with gas-phase H<sub>2</sub> (8). Some of the adsorbed CO dissociates irreversibly (7, 9) to form C<sub>s</sub> and O<sub>s</sub>. The atomic oxygen produced in this manner reacts rapidly with H<sub>s</sub> to form water, whereas the atomic carbon reacts with hydrogen to form CH<sub>x</sub> (x = 1-3) species (9, 10). The CH<sub>3,s</sub> species can react with additional hydrogen to form CH<sub>4</sub> or react with a CH<sub>2,s</sub> species, thereby initiating the process of chain growth. Chain propagation is sustained by CH<sub>2,s</sub> addition to adsorbed alkyl species. Chain termination can occur by hydrogen addition to a surface alkyl species to give a paraffin or by hydrogen abstraction to give an olefin.

A number of investigators have used isotopic-tracer techniques to identify the species involved in the chain growth process and to estimate the rate coefficients for chain propagation and termination (7, 11-20). In studies conducted with a Ru/SiO<sub>2</sub> catalyst, Kobori *et al.* (11) concluded that hydrocarbons are formed

by the polymerization of  $\text{CH}_x$  intermediates, and that CO insertion plays no part in the chain growth process leading to hydrocarbons. Work by Biloen *et al.* (12) on unsupported Co, Ni/SiO<sub>2</sub> and Ru/ $\gamma$ -Al<sub>2</sub>O<sub>3</sub> has shown that carbidic intermediates are involved in the reaction and that methane and higher hydrocarbons have a common precursor. Stockwell *et al.* (17) were unable to conclude whether chain growth occurred via a CO or a  $\text{CH}_x$  insertion mechanism. Studies on an Fe/Al<sub>2</sub>O<sub>3</sub> catalyst by Stockwell *et al.* (18) implicated a CH species as responsible for chain growth. They concluded that once chain growth is initiated, methane and higher hydrocarbon production is rapid and hence, coverages by the growing chains is small.

Several attempts to determine the rate coefficients for chain propagation and termination have been reported. Zhang and Biloen (14) have looked at the successive incorporation of <sup>13</sup>C into C<sub>1-3</sub> hydrocarbon products over Co and Ru catalysts. For Co, it was estimated that at 483 K, the value of the apparent rate constant for propagation decreased from 0.045 to 0.025 s<sup>-1</sup> and the corresponding value of the apparent rate constant for chain termination increased from 0.02-0.04 s<sup>-1</sup>, as the D<sub>2</sub>/CO ratio increased from 1 to 6.55. For the same reaction conditions, the coverage by alkyl chains was estimated to be between 0.19 and 0.25 ML, whereas the coverage by monomeric species was much smaller. For Ru, the apparent rate coefficient for chain propagation was estimated to be  $\geq 1\text{s}^{-1}$ . Based on similar experiments, Mims *et al.* (15) have estimated the apparent rate coefficient for chain propagation to be 2-4 s<sup>-1</sup> for a promoted Fe catalyst at 510 K and a H<sub>2</sub>/CO ratio of 1 (15), and 2 s<sup>-1</sup>

on Co at 475 K and a  $H_2/CO$  ratio of 2 (16). Over both Fe and Co, the coverage by the monomeric species exceeded the coverage by hydrocarbon chains. In a recent study using a Ru/TiO<sub>2</sub> catalyst, Yokomizo and Bell (21) observed that 80 % of the carbidic species on the Ru surface served as a monomer building block, and 20 % acted as the precursor to methane. The rate coefficient for chain termination was estimated to be 0.044 s<sup>-1</sup> at T = 463 K,  $p_{CO} = 50$  torr and a  $D_2/CO = 3$ . The total coverage by C<sub>1</sub> species was reported to be 0.25 ML, and the coverage by C<sub>2+</sub> species leading to hydrocarbon product was estimated at 0.1 ML.

The objective of the present investigation is to estimate the rate coefficients for chain initiation, propagation and termination, and to study their dependence on temperature and  $D_2/CO$  ratio. A further aim of this effort is to determine the surface coverages by the various reactive carbonaceous species present on the catalyst. A Ru/TiO<sub>2</sub> catalyst was used for these investigations because of the high specific activity of Ru for FTS and its characteristically high value of  $\alpha$  (22). The absence of alcohols from the products of FTS over Ru was a further reason for choosing this metal. Titania was used to support and disperse the ruthenium since titania-supported Group VIII metals are known to be more active than silica- or alumina-supported Group VIII metals (23-26).

## 2.0 EXPERIMENTAL

### 2.1 Catalyst Preparation and Characterization

A 3.3% Ru/TiO<sub>2</sub> catalyst was prepared by incipient wetness

impregnation of Degussa P-25 titania with an aqueous solution of  $\text{RuCl}_3 \cdot \text{H}_2\text{O}$  (Strem). Details of the preparation are given in ref. (27). The dried catalyst was reduced at 503 K to minimize encapsulation of the Ru crystallites by titania. The metal content of the catalyst was determined by X-ray fluorescence. The chloride level after reduction was below the detection limit (0.02%). The dispersion of Ru was determined by  $\text{H}_2$  chemisorption to be 15.5%, while the CO uptake on the freshly reduced catalyst was 1.3 ML (ML based on  $\text{H}_2$  chemisorption). The BET surface area, determined from a  $\text{N}_2$  isotherm at 77 K, was 47.5  $\text{m}^2/\text{gm}$ .

## 2.2 Apparatus

$\text{D}_2$ ,  $^{12}\text{CO}$ ,  $^{13}\text{CO}$  and He were supplied from a gas manifold to a low dead volume quartz microreactor. UHP  $\text{H}_2$  (Matheson Gas) or  $\text{D}_2$  (Union Carbide) were further purified by passage through a Deoxo unit (Engelhard Industries) and water was removed by a molecular sieve 13X trap. UHP CO (99.999% pure, Matheson Gas) was passed through a glass bead trap maintained at 573 K to remove iron carbonyls, an Ascarite trap to remove  $\text{CO}_2$ , and a molecular sieve trap to remove water. UHP He was passed through a molecular sieve trap to remove water.  $^{13}\text{CO}$  (Isotec Inc, 99%  $^{13}\text{C}$ ) was used as supplied.

Tylan mass flow controllers were used to regulate the flow of all four gases. The  $^{12}\text{CO}$  and  $^{13}\text{CO}$  streams flow from the flow controllers into two separate low dead-volume, 2-position, 4-port valves. One stream from each of these valves flows through a

bubbler to a vent line, while the other stream flows to a 4-way tee. He and D<sub>2</sub> are mixed and introduced into the third inlet of the 4-way tee, and the outlet from the tee goes to the microreactor. This flow scheme enables establishment of steady-state flow to the vent line in both CO streams and allows switching the reactor feed from one isotopically labeled form of CO to the other without significant flow perturbation. By simultaneous switching of the two 4-port valves, one avoids the elution of a small slug of the first isotope of CO held up in the valve and flow line.

### *2.3 Product Analysis*

The steady-state distribution of reaction products was determined by gas chromatography and the temporal variation in the distribution of <sup>12</sup>C and <sup>13</sup>C in each product was determined by isotopic ratio gas chromatography-mass spectroscopy (28-30). Figure 1 shows a schematic of the analytical system. A 10-port GC sampling valve (Valco E410UWP) and a multiposition 16 sample-loop valve (Valco E6ST16T) were used to acquire and store samples. Both valves are housed in valve ovens and can be actuated electrically. Flow lines downstream of the reactor, the valve ovens and lines to the GC inlet were all maintained at 393 K, to minimize product condensation.

Product analysis is initiated by injecting the contents of one of the sample loops into a Perkin-Elmer Sigma 3B chromatograph containing a fused silica capillary column (0.25mm i.d. x 50 m)

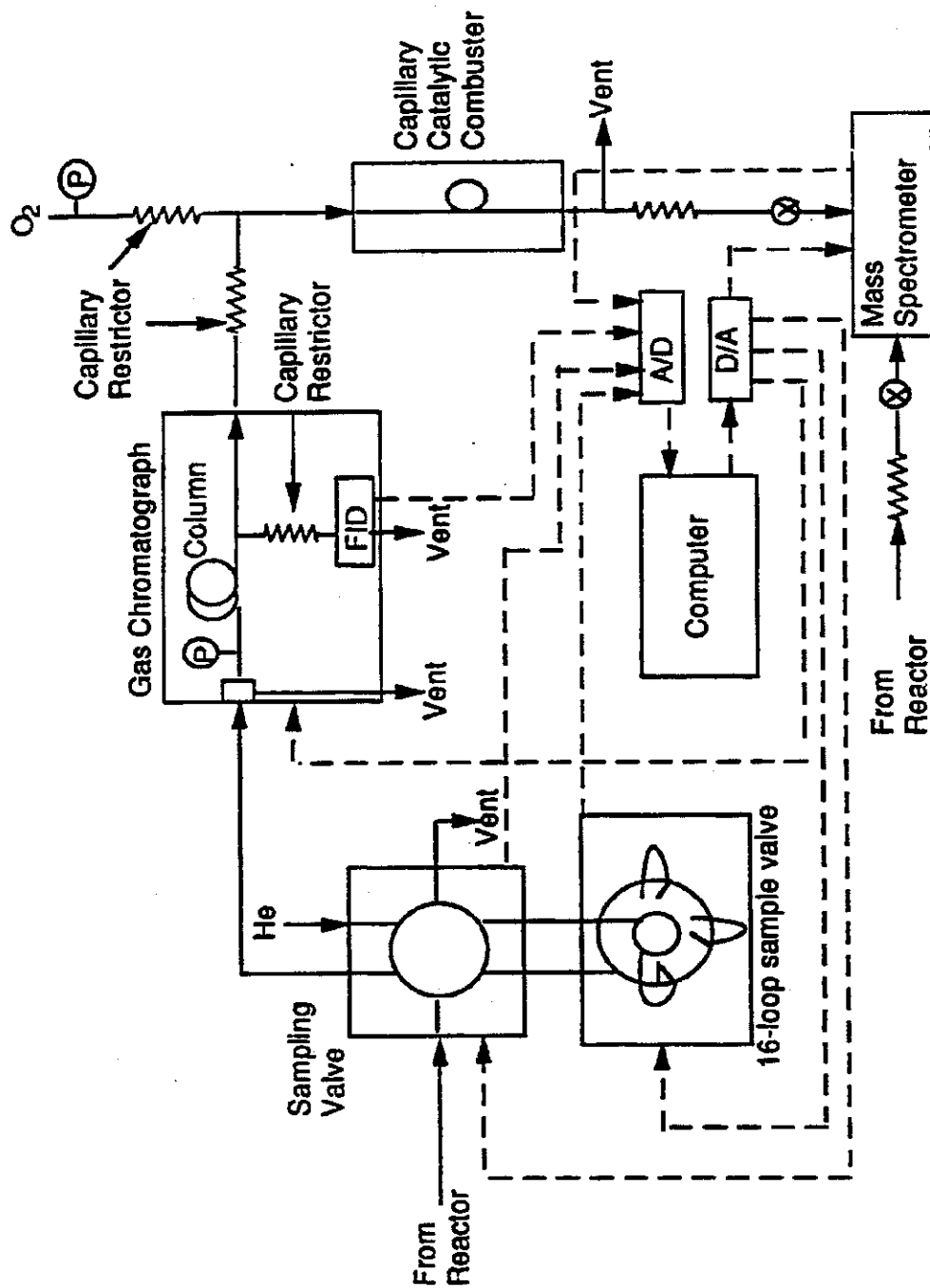


Fig. 1 Schematic of Analytical System

coated with a 1  $\mu\text{m}$  film of SE-54. To achieve good product resolution, the column is maintained at 233 K for 4 min, then ramped at 20 K/min to 523 K, and finally held at 523 K for 10 min. This sequence results in a total sample analysis time of 28.5 min.  $\text{C}_{1-2}$  products elute at the initial temperature,  $\text{C}_{3-8}$  products elute during the temperature ramp, and  $\text{C}_{9-18}$  products elute at the final temperature. Products heavier than  $\text{C}_{14}$  hydrocarbons are not detected. The column effluent is split into two streams using a glass-lined capillary union (SGE); one line (0.11 mm i.d.) is sent to an FID detector for quantification, while the other transfer line (0.20 mm i.d.) is routed to a capillary combustor. This latter stream is mixed with  $\text{O}_2$  and combusted to  $\text{CO}_2$  in a 2 m long capillary (0.2 mm i.d.) containing Pt wire (0.13 mm o.d.) maintained at 873 K. Details of the capillary combustor are given in ref. (30).

The effluent from the combustor is leaked into a vacuum chamber containing the probe of a UTI 100C quadrupole mass spectrometer. The leak is accomplished by coupling the exit of the combustor directly to the inlet capillary restrictor of the mass spectrometer. The flow rate through the combustor is sufficient to preclude the back diffusion of air into the mass spectrometer. Complete combustion of all hydrocarbon products except methane was confirmed by the absence of peaks at masses corresponding to fragments derived from the hydrocarbons. The combustion of methane was found to be inhibited by the presence of a large amount of  $\text{CO}$ , which elutes at the same time as methane. The masses monitored by the mass spectrometer were amu 4 (He), amu 20 ( $\text{D}_2\text{O}$ )

and  $^{12}\text{CD}_4$ ), amu 21 ( $^{13}\text{CD}_4$ ), amu 44 ( $^{12}\text{CO}_2$ ) and amu 45 ( $^{13}\text{CO}_2$ ). The distribution of  $^{12}\text{C}$  and  $^{13}\text{C}$  in methane was determined from the relative intensities of the signals for amu 20 and amu 21. The presence of  $\text{D}_2\text{O}$  in the products, which also produces a signal at amu 20, did not interfere with the detection of  $^{12}\text{CD}_4$ , since  $\text{CD}_4$  and  $\text{D}_2\text{O}$  elute at sufficiently different times. The distribution of  $^{12}\text{C}$  and  $^{13}\text{C}$  in  $\text{C}_{2+}$  hydrocarbons was obtained from the relative signal intensities at amu 44 and amu 45. The temporal resolution of these products recorded by the mass spectrometer was comparable to that recorded by the FID.

Operation of the sampling valves was controlled by an IBM PC/XT computer programmed to acquire samples at preset times. The output from the FID detector and mass spectrometer were acquired by the computer at the rate of 2 data points a second.

#### 2.4 Procedure

Experiments were carried out at temperatures between 453 K and 483 K. The ratio of  $\text{D}_2/\text{CO}$  was varied between 2 and 5, by holding the CO partial pressure at 0.1 atm, and varying the  $\text{D}_2$  partial pressure between 0.2 and 0.5 atm. The total flowrate to the reactor was  $100 \text{ cm}^3/\text{min}$ . CO conversions were maintained as low as possible and, in most cases, were below 10%. For each set of conditions, the reaction was allowed to proceed in a mixture of  $^{12}\text{CO}$ ,  $\text{D}_2$  and He for 20 min, to avoid the rapid initial loss in activity after start-up (27). Deactivation after the initial start-up proceeds with a first order decay time constant of 5 h. After each

experiment, the catalyst was reduced in  $D_2/He$  at 523 K for 2 h to ensure that steady-state activity levels were maintained.

Isotopic-tracer, transient response experiments were initiated by switching the feed from a stream containing  $^{12}CO$  to one containing an equivalent concentration of  $^{13}CO$ , after steady-state conditions had first been achieved in  $^{12}CO$ . In this fashion, the steady-state activity of the catalyst was not perturbed by the switch in isotopic composition of the CO. To obtain good temporal resolution of the isotopic composition of the products, the following sampling sequence was used. A sample was taken 15 s after the switch in CO isotopic composition, followed by four samples taken at 10 s intervals, followed by a sample taken after an interval of 15 s, one taken after an interval of 20 s, one taken after an interval of 30 s interval, and two taken after intervals of 240 s. In this way, 11 samples are acquired in 10 min. Because the fill-time of the sample loops is 6s, data were not collected at intervals shorter than 10s. Since most changes in product isotopic composition occur in the first 2 min after the switch in feed isotopic composition, it is desirable to acquire data at intervals shorter than 10 s. To do so, the feed composition was changed from  $^{13}CO/D_2/He$  to  $^{12}CO/D_2/He$  and 5 samples were acquired at 10 s intervals for upto 60 s.

Figure 2 is a schematic of the data acquired during a typical experiment. The curves labelled  $F(^{12}C)$  and  $F(^{13}C)$  represent the fractions of the carbon atoms that are  $^{12}C$ -labelled and  $^{13}C$ -labelled, respectively.  $F(^{12}C)$  is calculated by dividing the  $^{12}C$  concentration observed at a given time by the initial steady-state  $^{12}C$

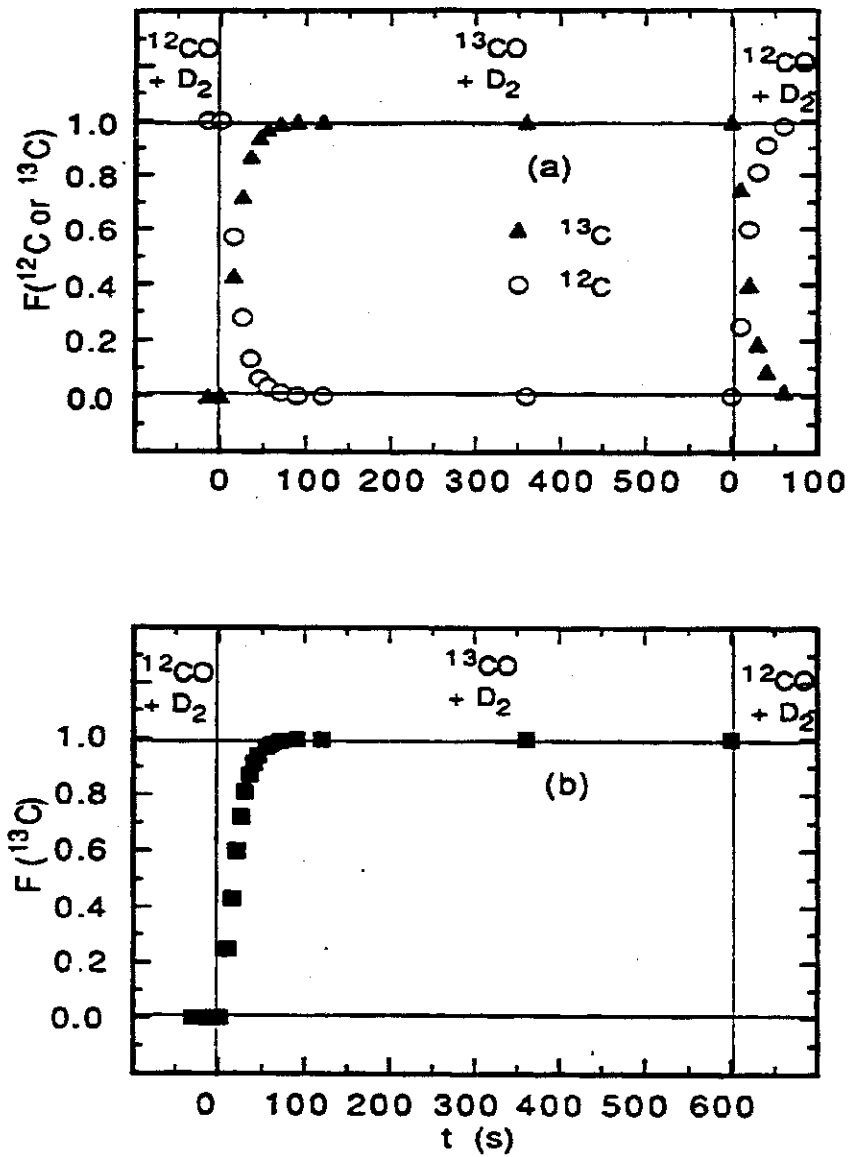


Fig. 2 (a) Isotopic Transient Data Sampling.  
(b) Average Rise Curve.

concentration measured in  $^{12}\text{CO}/\text{D}_2$ ;  $F(^{13}\text{C})$  is obtained by dividing the observed  $^{13}\text{C}$  concentration by the  $^{13}\text{C}$  concentration measured after 10 min in  $^{13}\text{CO}/\text{D}_2$ . [It had previously been determined that the transients are complete in 10 min.] The sum of  $F(^{12}\text{C})$  and  $F(^{13}\text{C})$  for a given product always equals 1.0. For the first portion of the experiment, the rise curve points for each product were calculated as the average of the values of  $F(^{13}\text{C})$  and  $[1-F(^{12}\text{C})]$ , and in the latter section, as the average of the values of  $F(^{12}\text{C})$  and  $[1-F(^{13}\text{C})]$ . All the points could then be combined to give a rise curve with 16 points. Sampling times were chosen such that data could effectively be collected at 5 s intervals for the first minute after the switch. Data acquired during the initial part of the experiment, as the  $^{13}\text{C}$  content in the product rises, was found to be in agreement with data from the latter part of the transient experiment, when the  $^{13}\text{C}$  content in the products declines.

### 3.0 THEORETICAL MODELLING

#### 3.1 Chain growth model

Simulation of the experimentally observed transients was carried out on the basis of the scheme shown in Fig. 3. This scheme is identical to that used by Zhang and Biloen (14) and by Mims and McCandlish (16). In Fig. 3,  $\text{CO}_g$  and  $\text{CO}_s$  refer to gas-phase and adsorbed CO,  $C_{m,s}$  refers to adsorbed monomeric building units and  $C_{n,s}$  and  $C_{n,g}$  refer to adsorbed alkyl chains and gaseous products containing  $n$  carbon atoms. Reference to reactions 1-16 in the

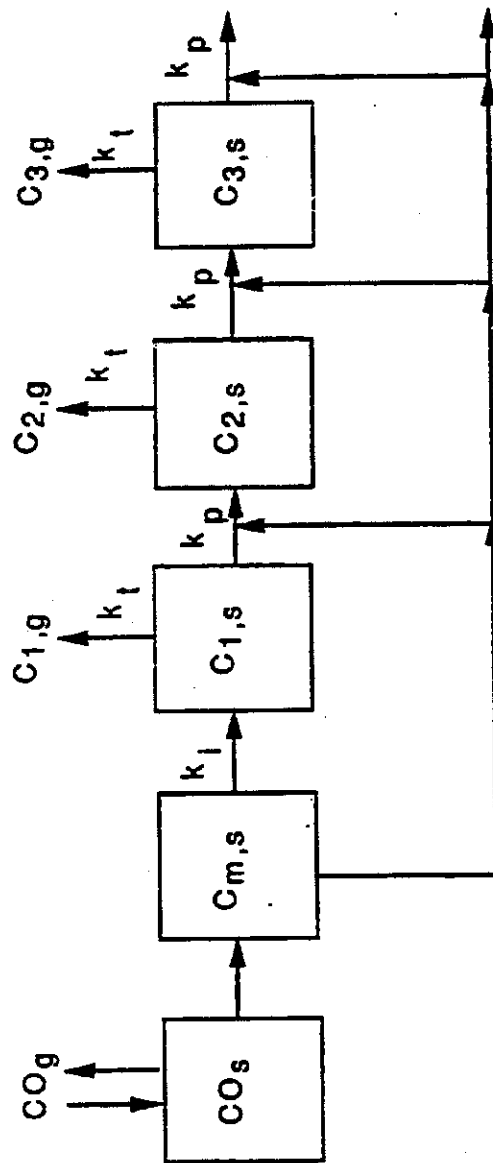


Fig. 3 Chain Growth Model

Introduction show that the scheme in Fig. 3 represents a simplification of the more detailed reaction sequence. First, the species  $C_s$ ,  $CH_s$  and  $CH_{2,s}$  are treated as a common species,  $C_m$ , on the assumption that the individual species are in equilibrium with each other. Second, no distinction is made between chain termination to olefins and paraffins. The rate coefficient for conversion of  $C_{m,s}$  to  $C_{1,s}$  is the apparent first-order rate coefficient for chain initiation,  $k_i$ . The rate coefficients  $k_p$  and  $k_t$ , are first-order rate coefficients for chain propagation, and termination. The dependence of any process on adsorbed hydrogen is not shown explicitly, since, for a given set of reaction conditions, the surface coverage of hydrogen is time independent.

### 3.2 Steady-State Rate and Label Balances

The scheme presented in Fig. 3 can be used to derive expressions for  $F_m$  and  $F_n$ , the fraction of labelled carbon in the monomer pool and in the pool of chains of length  $n$ , respectively. Equations for  $F_m$  and  $F_n$  are obtained in the following manner. A balance on labelled carbon entering and leaving the monomer pool gives

$$\theta_m \frac{dF_m}{dt} = k_d \theta_{CO} F_{CO} - \theta_m F_m (k_i + k_p \sum_{n=1}^{\infty} \theta_n) \quad (1)$$

[In eqn. 1,  $\theta_{CO}$ ,  $\theta_m$ , and  $\theta_n$  are the surface coverages for CO, monomeric building units,  $C_{m,s}$ , and alkyl chains,  $C_{n,s}$ , respectively.]

At steady state,

$$N_{CO} = k_d \theta_{CO} = k_i \theta_m + k_p \theta_m \sum_{n=1}^{\infty} \theta_n \quad (2)$$

Combining eqns. (1) and (2), one obtains

$$\frac{dF_m}{dt} = \frac{F_{CO} - F_m}{\tau_m} \quad (3)$$

where  $\tau_m = 1/(k_i + k_p(\sum \theta_n))$

The appearance and disappearance of labelled carbon in the methane precursor pool  $C_1$  is governed by

$$\theta_1 \frac{dF_1}{dt} = k_i \theta_m F_m - k_t \theta_1 F_1 - k_p \theta_m \theta_1 F_1 \quad (4)$$

Since at steady state

$$k_i \theta_m = k_t \theta_1 + k_p \theta_m \theta_1 \quad (5)$$

eqn. (4) can be rewritten as

$$\frac{dF_1}{dt} = \frac{F_m - F_1}{\tau} \quad (6)$$

where  $\tau = 1/(k_p \theta_m + k_t)$ . The appropriate balance on labelled carbon in the pool of alkyl species containing  $n$  carbon atoms is given by

$$n \theta_n \frac{dF_n}{dt} = k_p \theta_m \theta_{n-1} [(n-1)F_{n-1} + F_m] - k_p \theta_m \theta_n (nF_n) - k_t \theta_n (nF_n) \quad (7)$$

Once again, at steady state,

$$k_p \theta_m \theta_{n-1} = k_p \theta_m \theta_n + k_t \theta_n \quad (8)$$

so that eqn. 7 can be rewritten as

$$\frac{dF_n}{dt} = \frac{(n-1)F_{n-1} + F_m - F_n}{\tau} \quad (9)$$

The initial conditions for  $F_m$ ,  $F_1$ , and  $F_n$  are  $F_m = F_1 = F_n = 0$  at  $t = 0$ .

Since CO is assumed to equilibrate rapidly with the catalyst

surface,  $F_{CO} = 1$  for  $t \geq 0$ . With these initial conditions, the solution to eqn. 6 is

$$F_m(t) = 1 - \exp(-t/\tau_m) \quad (10)$$

An analytical solution for  $F_n(t)$  can be obtained using Laplace transforms and the convolution theorem (31). The resulting expression is

$$F_n(t) = 1.0 + \left( \frac{\exp(-\frac{t}{\tau_m})}{n} \right) \sum_{i=1}^n (-1)^{i-1} \left( \frac{\tau_m}{\tau - \tau_m} \right)^i + \left( \frac{\exp(-\frac{t}{\tau})}{n} \right) \sum_{i=1}^n \frac{1}{\tau^i} \sum_{r=0}^{i-1} \frac{t^{i-r-1}}{(i-r-1)!} \tau^{r+1} \left( \left( -\frac{\tau_m}{\tau - \tau_m} \right)^{r+1} - 1 \right) \quad (11)$$

## 4.0 RESULTS AND DISCUSSION

### 4.1 Catalyst Activity and Selectivity

Gas chromatographic analyses of the products taken during the isotopic transient experiments shows that the catalyst activity and selectivity are unchanged over the 11-min duration of the experiment. The main products observed are  $\alpha$ -olefins, cis- and trans- $\beta$ -olefins and n-paraffins. A few branched products are also detected, but these constitute less than 10% of the total product. Alcohols and other oxygenates are not detected. Mass spectrometric analysis of the products indicates that no  $CO_2$  is formed and that  $D_2O$  is the only oxygenated product.

Figure 4 shows an Anderson-Schulz-Flory (ASF) plot of the turnover frequencies for  $C_1$ - $C_{12}$  at 463K and a  $D_2/CO = 3$ . As is characteristic of Ru catalysts (3, 30), the points for  $C_2$  and  $C_3$

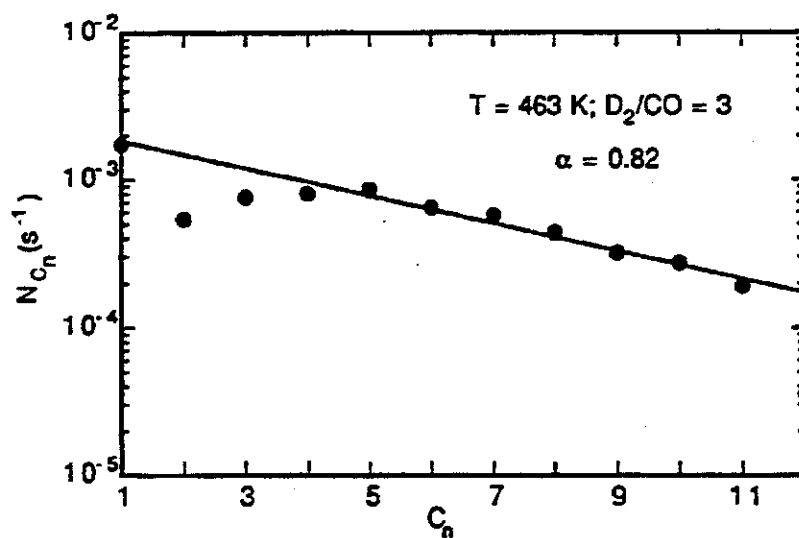


Fig. 4 Anderson-Schulz-Flory plot,  $\log N_{C_n}$  vs Carbon number, where  $N_{C_n}$  is the turnover frequency for products of carbon number  $n$ .

products fall below the line passing through the points for the C<sub>4</sub>-C<sub>11</sub> products. From the slope of this line,  $\alpha$  is determined to be 0.82.

Figures 5a and 5b show the dependence of the turnover frequency for CO consumption and  $\alpha$  on temperature, respectively.  $N_{CO}$  is calculated as  $\sum nN_{C_n}$  for values of  $n$  between 1 and 13, and  $\alpha$  is taken as the slope of the linear portion of the ASF plot. It is seen from Fig. 5a that  $N_{CO}$  exhibits an Arrhenius behavior for temperatures below 473 K, and then becomes nearly constant at higher temperatures. Calculations of the Weisz parameter indicate the absence of intraparticle mass transfer limitations, leading to the conclusion that the observed dependence on temperature is a reflection of the intrinsic kinetics. Figure 5b shows that  $\alpha$  decreases monotonically from 0.88 to 0.73 as temperature increases from 453K to 498K.

The effects of D<sub>2</sub> partial pressure on  $N_{CO}$  and  $\alpha$ , for a fixed temperature and CO partial pressure are shown in Figs. 6a and 6b. The value of  $N_{CO}$  is seen to increase linearly with increasing D<sub>2</sub> partial pressure, whereas the value of  $\alpha$  decreases monotonically. The trends reported in Figs. 5b and 6b are similar to those observed previously for Ru/Al<sub>2</sub>O<sub>3</sub> (3) and for supported Fe catalysts (4, 5).

Figure 7 shows a series of product selectivity plots. It is observed that the total straight-chain olefin/n-paraffin ratio rises from C<sub>2</sub> to C<sub>4</sub> and then decreases with increasing carbon number. The fraction of internal olefins in the straight-chain olefin product rises with increasing carbon number. The  $\beta$ -olefin fraction in the

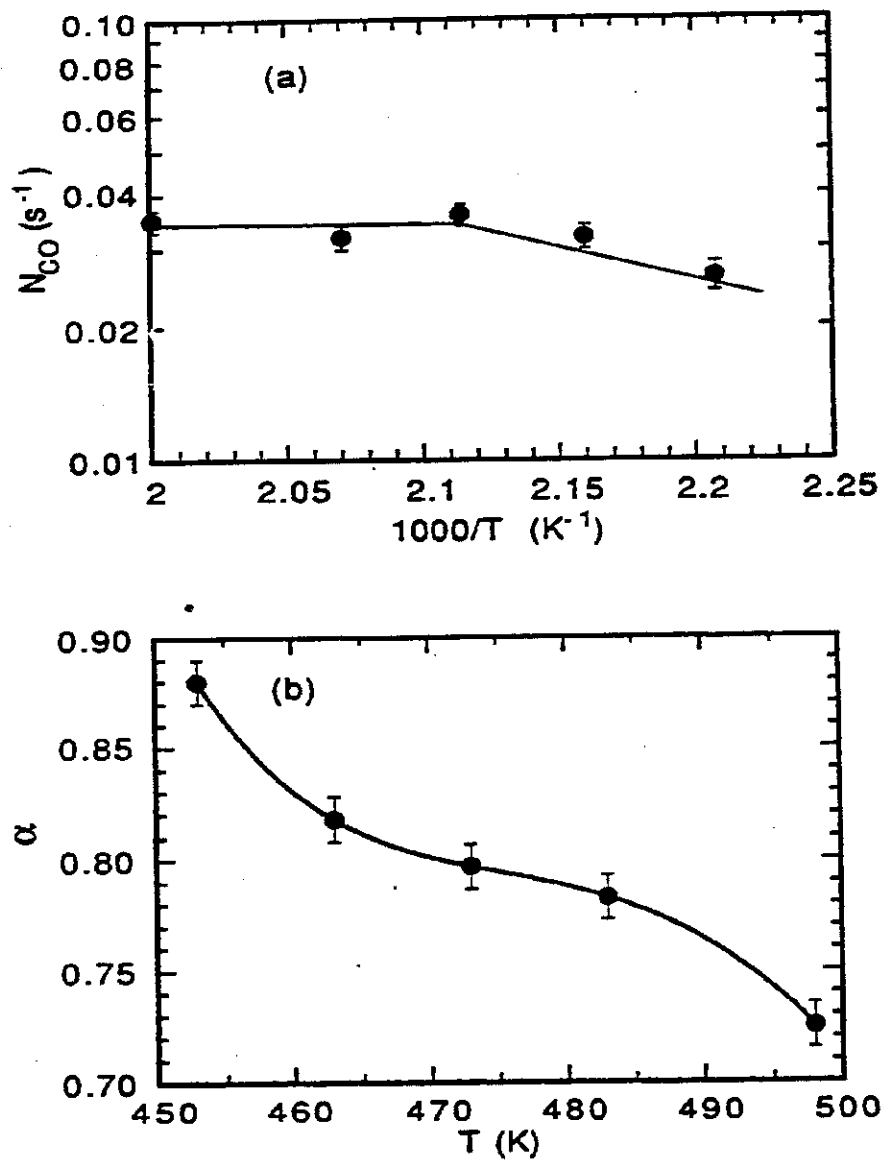


Fig. 5 a) CO turnover frequency,  $N_{CO}$ , as a function of temperature; (b) Chain growth parameter  $\alpha$  as a function of temperature;  $D_2/CO = 3$ .

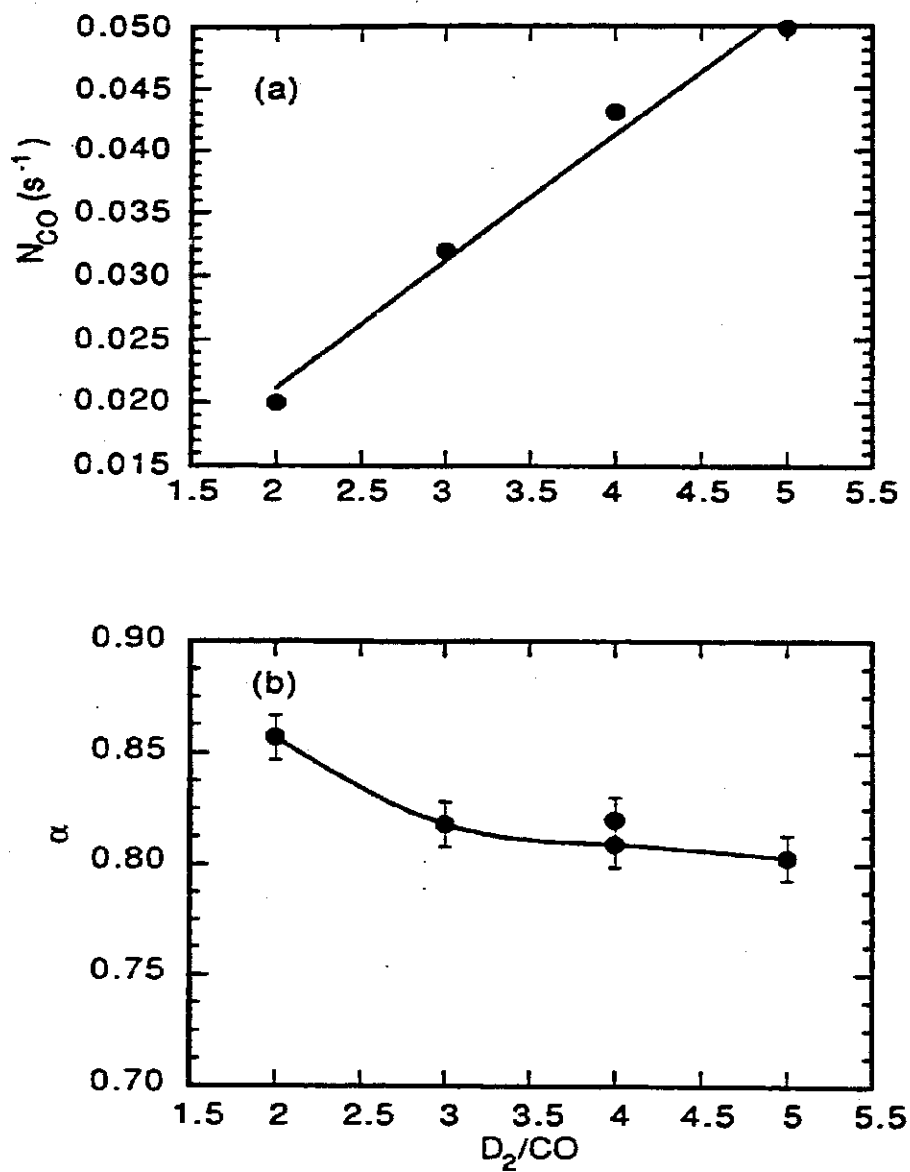


Fig. 6 (a) CO turnover frequency,  $N_{CO}$ , as a function of  $D_2/CO$  ratio; (b) Chain growth parameter  $\alpha$  as a function of  $D_2/CO$  ratio;  $T = 463$  K.

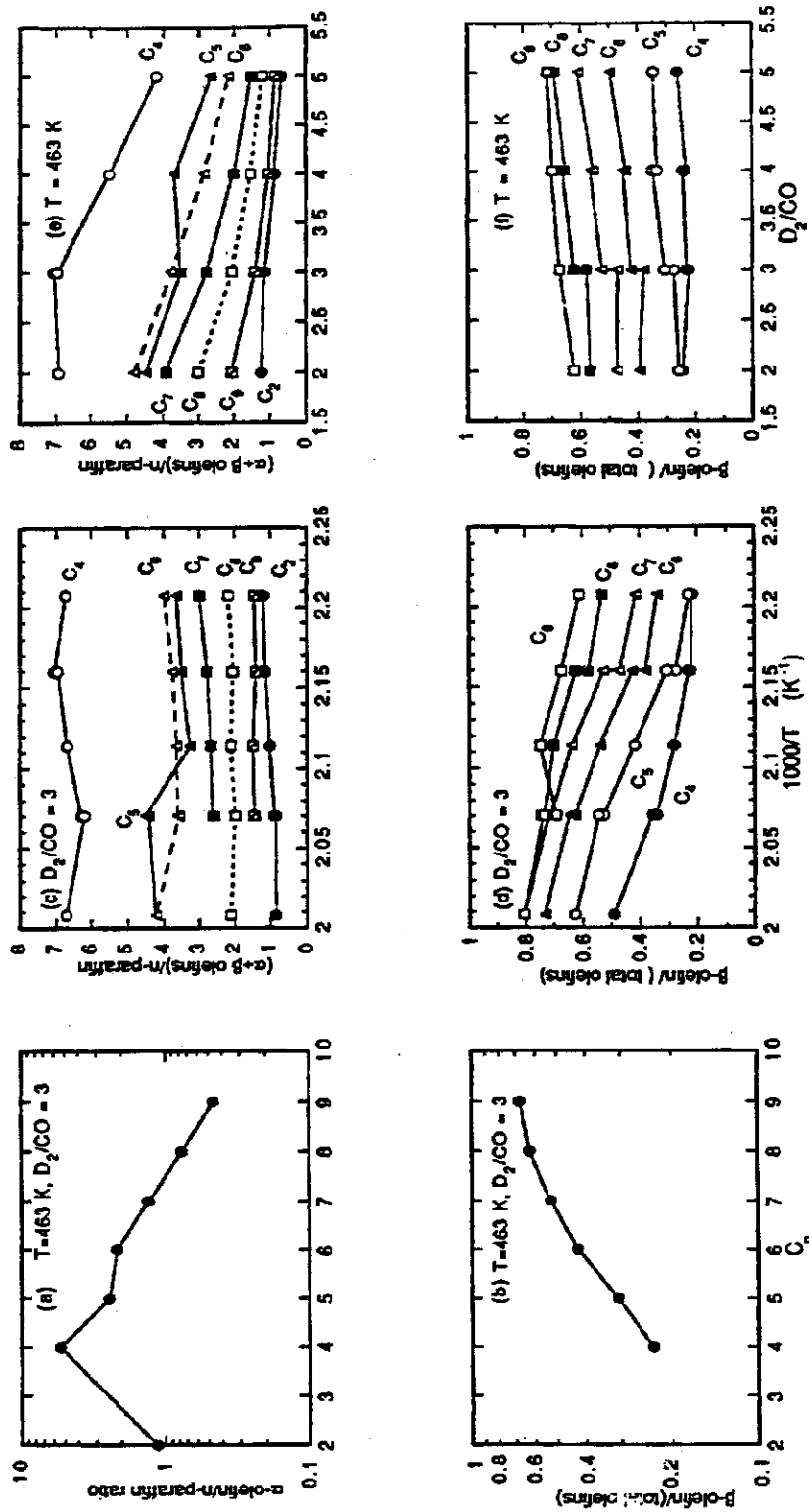


Fig. 7 (a)  $\alpha$ -olefin to n-paraffin ratio vs Carbon Number; (b)  $\beta$ -olefin fraction in straight-chain olefins vs Carbon Number; T = 463 K, D<sub>2</sub>/CO = 3; (c) Straight chain olefins to n-paraffin ratio as a function of temperature; (d)  $\beta$ -olefin fraction in straight-chain olefins as a function of temperature; D<sub>2</sub>/CO = 3; (e) Straight chain olefins to n-paraffin ratio as a function of D<sub>2</sub>/CO ratio; (f)  $\beta$ -olefin fraction in straight-chain olefins as a function of D<sub>2</sub>/CO ratio; T = 463 K.

olefin product at any carbon number also increases with temperature. The ratio of olefins to paraffins decreases with increasing  $D_2/CO$  ratio. These changes in product selectivity are in agreement with data reported by Dictor and Bell (32) on an Fe catalyst and by Schulz (33) on a Fe/Mn catalyst.

#### 4.2 *Isotopic Transients*

The incorporation of  $^{13}C$  and the concurrent decline in  $^{12}C$  in the  $C_1$  and  $C_{3-8}$  products was monitored by isotope-ratio GC-MS, following a switch in the feed from  $^{12}CO/D_2$  to  $^{13}CO/D_2$ . The concentration of the  $C_2$  product was too low for mass spectrometric detection. Figures 8 and 9 show representative plots of  $F_1(t)$  and  $F_n(t)$  ( $n = 3-8$ ), respectively. The data points in Fig. 8 are based on the measured isotopic fractions in all olefins and paraffins of a given carbon number, since it was observed that the dynamics for products with a given number of carbon atoms could not be differentiated on the basis of structure (i.e., olefin vs paraffin,  $\alpha$ -olefin vs  $\beta$ -olefin, n-paraffin vs branched paraffin). Figure 8 shows that the methane transient rises rapidly but on comparison with Figure 9, does not lie before the  $C_3$  data. The transients for  $C_{3+}$  are shown in Fig. 8 and are seen to approach 1.0 after 120 s. While there is considerable scatter in the data, it is observed that the appearance of  $^{13}C$ -labelled carbon in the products is progressively slower as the value of  $n$  increases from 3 to 8. This trend is particularly evident for the  $C_{6+}$  products.

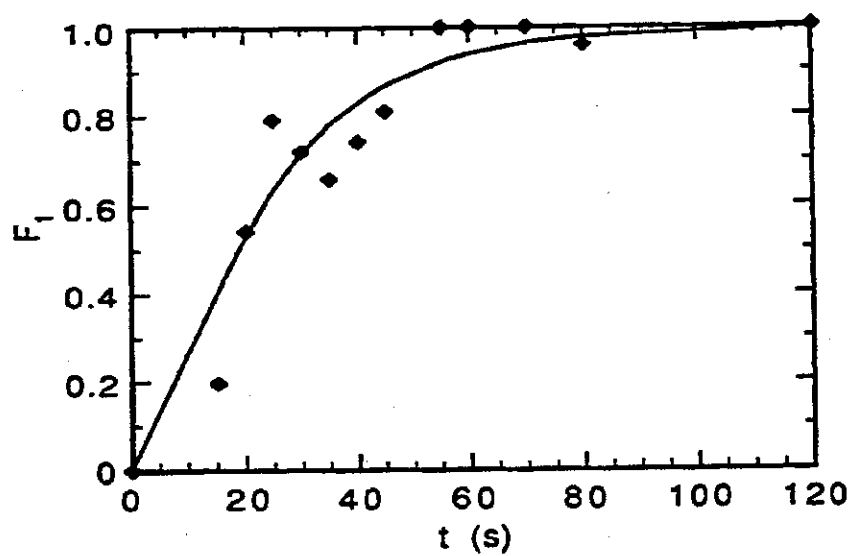


Fig. 8  $F(^{13}\text{CD}_4)$  rise after a switch from  $^{12}\text{CO}/\text{D}_2$  to  $^{13}\text{CO}/\text{D}_2$  at  $t = 0$ .  $T = 463 \text{ K}$ ,  $\text{D}_2/\text{CO} = 3$ .

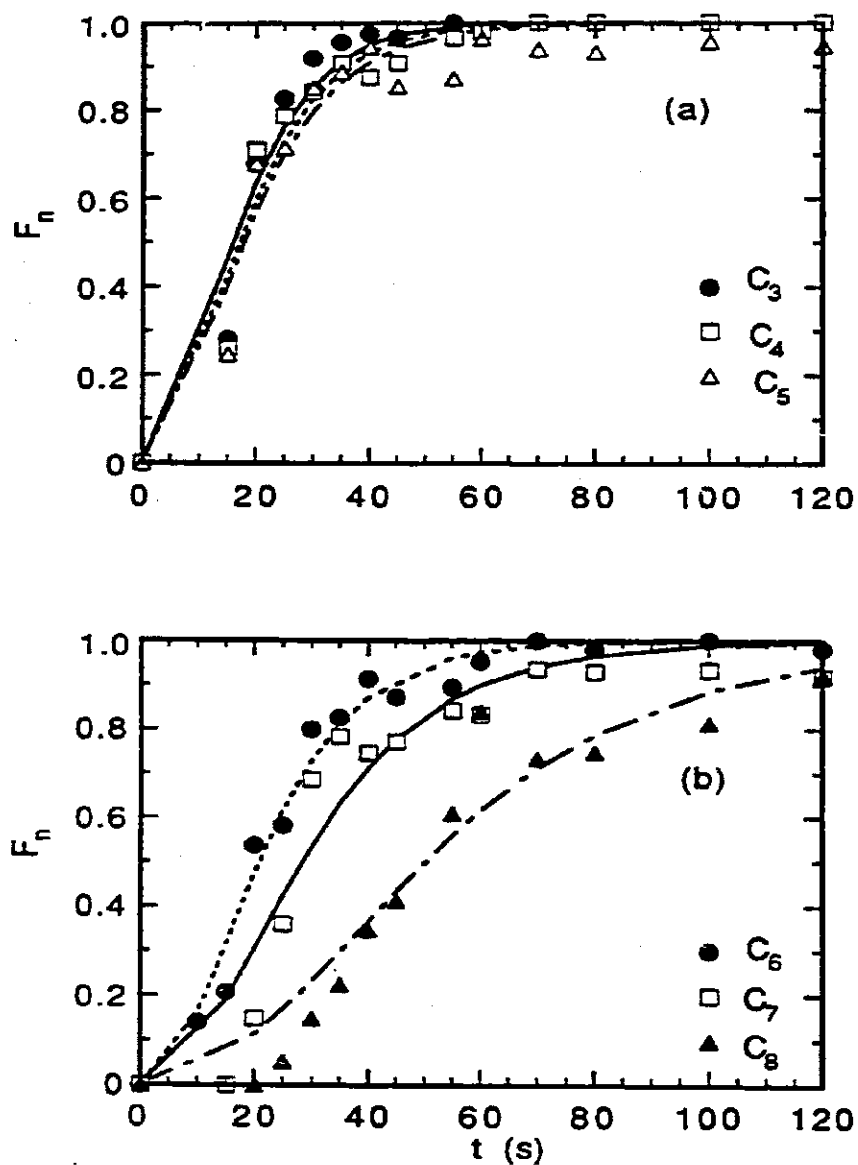


Fig. 9 (a)  $F(^{13}\text{C})$  rise in the  $C_3$ - $C_5$  products; (b)  $F(^{13}\text{C})$  rise in the  $C_6$ - $C_8$  products; transient response after a switch from  $^{12}\text{CO}/\text{D}_2$  to  $^{13}\text{CO}/\text{D}_2$  at  $t = 0$ .  $T = 463$  K,  $\text{D}_2/\text{CO} = 3$ .

#### 4.21 Parameter evaluations

Values of the two parameters  $\tau$  and  $\tau_m$  were obtained by fitting the analytical expressions for  $F_n$  given by eqn. 11 to the experimental data. This was done using a quasi-Newton method (31) to minimize the objective function  $S_n(\tau, \tau_m)$  defined as

$$S_n(\tau, \tau_m) = \sum_{j=1}^M [F_n^{\text{expt}}(t_j) - F_n(t_j)]^2 \quad (12)$$

In eqn. 12,  $F_n^{\text{expt}}(t_j)$  and  $F_n(t_j)$  are the experimental and theoretical values at time  $t_j$  and  $M$  is the number of experimental points.

Figures 8 and 9 show data and model fits at a temperature of 463 K and a  $D_2/CO$  ratio of 3. The F-test was used to assess the statistical adequacy or lack of fit of the model (34, 35). For each value of  $n$ , the F-test indicated that the model fit the data at a 95% confidence interval. The parameters  $\tau$  and  $\tau_m$  were determined independently for each of the transients from  $C_1$ - $C_8$ . Table 1 shows values obtained for the data set at 463 K and  $D_2/CO = 3$ . It is evident that the values of  $\tau$  and  $\tau_m$  determined from different transients exhibit a modest spread in values. Of particular note are the large values for  $\tau_m$  for  $n = 1$  and  $n = 8$ . For  $n = 8$ , the value of  $\tau_m$  is directly related to the slow approach of  $F_8(t)$  to unity (see Fig. 8), as a consequence of a partial loss of product due to condensation in the transfer-line upstream of the capillary combustor. The large value of  $\tau_m$  for  $n = 1$  also reflects the slow approach of  $F_1(t)$  to unity. In part this may be due to the presence of  $^{12}C$  impurity in the  $^{13}CO$

TABLE 1

$\tau$  and  $\tau_m$  obtained from fitting the chain growth model to the data:  
 $D_2/CO = 3$ ;  $T = 463$  K.

Carbon Number	$\tau$ (s)	$\tau_m$ (s)
1	4.7	19.6
3	5.2	7.8
4	3.7	10.3
5	2.8	12.3
6	3.2	12.7
7	3.5	16.7
8	5.7	31.6
Average	$3.9 \pm 0.9^1$	$11.9 \pm 4.0^2$

<sup>1</sup> Average of values for C<sub>1</sub>, C<sub>3-7</sub>. See text for details.

<sup>2</sup> Average of values for C<sub>3-7</sub>.

feed. For these reasons, it was decided that average values of  $\tau$  should be based on the individual values obtained for  $C_1$  and  $C_{3+}$ , and average values of  $\tau_m$  should be based on individual values obtained for  $C_{3+}$ . It was found that the  $F_n$  predictions based on the average values of  $\tau$  and  $\tau_m$  were nearly indistinguishable from those based on the best-fit model values for each  $n$  from 3-7. Tables 2 and 3 show the average values of  $\tau$  and  $\tau_m$  obtained for the transients when temperature and the  $D_2/CO$  ratio were varied.

From Tables 2 and 3, it is seen that the modelling leads to the result that  $\tau < \tau_m$  and that the ratio  $\tau_m/\tau$  lies between 3 and 13. This is similar to the findings of Mims *et al.* (16) on  $Co/SiO_2$  and promoted Fe and is in disagreement with the results of Zhang and Biloen (14) on Co. This modelling result implies that active species on the surface spend a larger portion of their residence time in the monomer pool than in alkyl chains and further translates to higher coverages by the monomer pool than by the hydrocarbon precursors.

#### 4.22 Intrinsic Rate Parameters and Surface Coverages

The values of  $k_i$ ,  $k_p$ , and  $k_t$ , and  $\theta_m$  and  $\Sigma\theta_n$ , can be determined from the values of  $\tau$  and  $\tau_m$ , obtained through the fitting procedure described above, and the values of  $N_{CO}$ ,  $N_{Cn}$  and  $\alpha$ , obtained from steady-state rate data. The approach used to calculate the rate coefficients and the surface coverages is described in the Appendix. Table 4 gives a complete summary of all the results at 463 K and  $D_2/CO = 3$ .

TABLE 2

Average  $\tau$  and  $\tau_m$  obtained from fitting the chain growth model to the data:

$D_2/CO = 3$ ; temperature is varied.

T (K)	$\tau_{av}(s)$	$\tau_{m,av}(s)$
453	3.5	13.5
463	3.9	11.9
463	3.9	15.0
473	1.8	18.1
483	2.1	18.8
483	1.6	19.1

TABLE 3

Average  $\tau$  and  $\tau_m$  obtained from fitting the chain growth model to the data:

$D_2/CO$  ratio is varied;  $T = 463$  K

$D_2/CO$	$\tau_{av}(s)$	$\tau_{m,av}(s)$
2	3.3	14.0
3	3.9	11.9
4	1.5	16.7
4	2.5	15.2
5	2.5	13.1

TABLE 4

Transient at standard reaction conditions: Ru/TiO<sub>2</sub> catalyst.

Reaction T = 463 K; D<sub>2</sub>/CO = 3

N<sub>CO</sub> = 0.032 s<sup>-1</sup>; α = 0.82

τ = 3.9 s

k<sub>p</sub><sup>app</sup> = 0.212 s<sup>-1</sup>, 0.208 s<sup>-1</sup>

k<sub>t</sub> = 0.047 s<sup>-1</sup>, 0.046 s<sup>-1</sup>

k<sub>i</sub> = 0.022 s<sup>-1</sup>, 0.021 s<sup>-1</sup>

Σθ<sub>n</sub> = 0.14 ML, 0.17 ML

θ<sub>m</sub> = 0.38 ML, 0.48 ML

θ<sub>CO</sub> = 0.67 ML

( Two values indicate results of separate experiments.)

Figure 10 shows the variation of rate coefficients  $k_i$ ,  $k_p$ , and  $k_t$  with  $T^{-1}$ . The value of the initiation rate coefficient  $k_i$  appears to be independent of temperature. This trend can be rationalized if the initiation of chain growth is assumed to proceed via the process  $\text{CH}_{2,s} + \text{H}_s \rightarrow \text{CH}_{3,s}$ . In such a case,  $k_i$  is an apparent rate coefficient, representing the product of the true rate coefficient,  $k'_i$ , and the coverage of adsorbed hydrogen,  $\theta_H$ . Since  $k'_i$  is expected to increase with increasing temperature but  $\theta_H$  is expected to decrease, the product of  $k'_i$  and  $\theta_H$  should be less sensitive to temperature than either of the two factors making up the product. The plots of  $k_p$  and  $k_t$  versus  $T^{-1}$  both have negative slopes, from which it is determined that the activation energy for chain propagation,  $E_p$ , is 8 kcal/mol and the activation energy for chain termination,  $E_t$ , is 20 kcal/mol.

The present evaluation of  $k_p$  can be compared to the estimated apparent rate of propagation reported by Zhang and Biloen (14). To do so,  $k_p$  is multiplied by  $\theta_m$  (see below) to obtain  $k_p^{\text{app}} = k_p \theta_m$ . For the data presented in Fig. 10,  $k_p^{\text{app}}$  lies between 0.25 and 0.5 s<sup>-1</sup>. This range lies somewhat below Zhang and Biloen's estimate of >1 s<sup>-1</sup>. There is close agreement between the values of  $k_t$  reported here and in the work of Yokomizo *et al.* (21). Using a Ru/TiO<sub>2</sub> catalyst similar to that described here, Yokomizo *et al.* determined a value of  $k_t = 0.044 \text{ s}^{-1}$  at  $T = 463 \text{ K}$ , from modelling of temperature programmed surface reaction (TPSR) data. For the same reaction conditions, we obtain a value of  $k_t = 0.047 \text{ s}^{-1}$ .

The activation energy for chain termination (20 kcal/mol) is

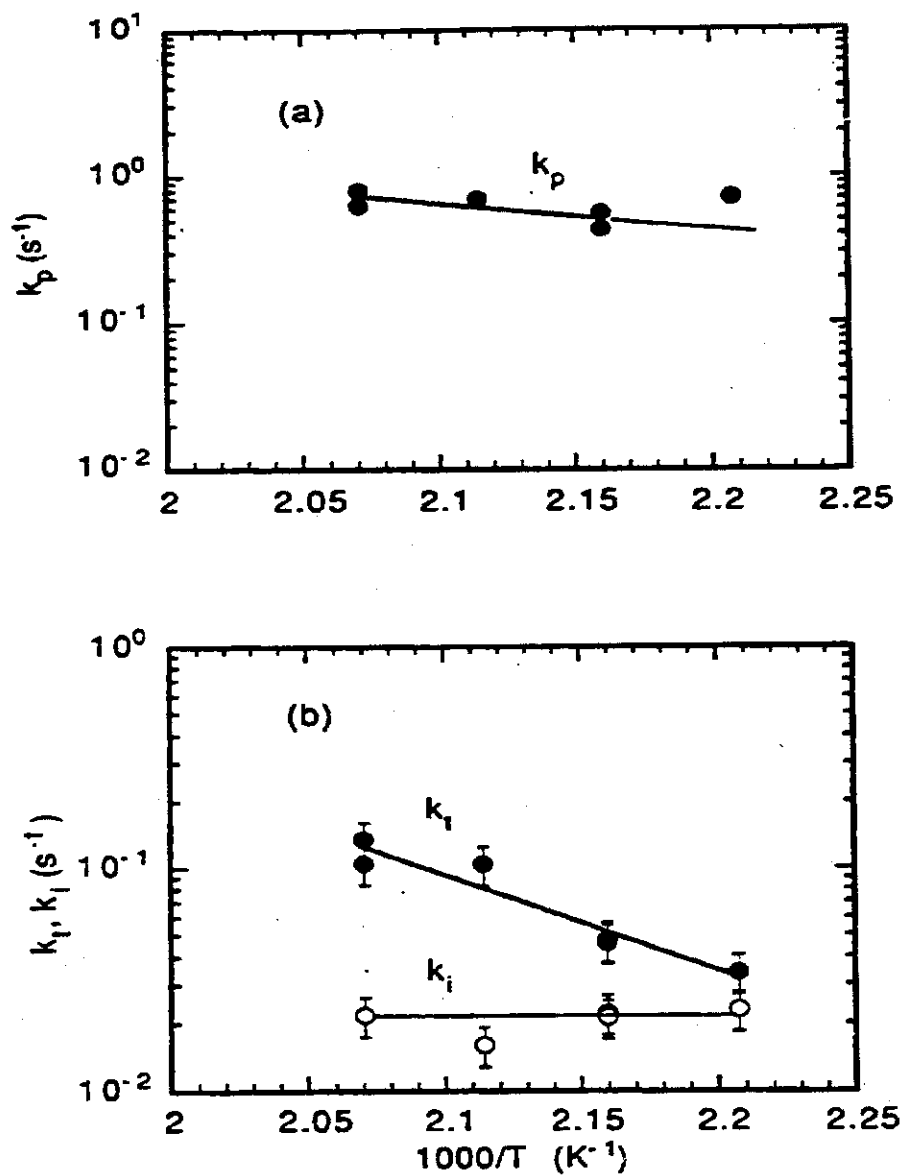


Fig. 10 (a) Propagation rate constant,  $k_p$ , as a function of temperature; (b) Initiation rate constant,  $k_i$ , and termination rate constant,  $k_t$ , as a function of temperature;  $D_2iCO = 3$ .

significantly higher than that for chain propagation (8 kcal/mol). This explains why the value of  $\alpha$  decreases with increasing temperature (see Fig. 5b). While experimental values of  $E_t$  and  $E_p$  have not been reported in the literature previously, Shustorovich and Bell (36) have shown using the Bond-Order-Conservation-Morse-Potential (BOC-MP) approach, that  $E_t$  should be larger than  $E_p$  for Ni and Fe. Thus, for Ni(111),  $E_p$  for the chain growth step to form a  $C_2$  species is estimated to be 6 kcal/mol, whereas  $E_t$  is estimated to be 11 kcal/mol for chain termination to ethylene and 19 kcal/mol for chain termination to ethane. For Fe(110),  $E_p$  for the formation of  $C_2$  species is estimated to be 20 kcal/mol, whereas  $E_t$  is estimated to be 16 kcal/mol for chain termination to ethylene and 32 kcal/mol for chain termination to ethane.

The effects of temperature on the calculated values of surface coverage by carbonaceous species is given in Fig. 11 and Table 5. The values of  $\theta_m$  lies between 0.3 and 0.6 ML, while the value of  $\Sigma\theta_n$  lies between 0.12 and 0.05 ML. It is observed that with increasing temperature,  $\theta_m$  increases, but  $\theta_t$  and  $\Sigma\theta_n$  decrease. These trends are consistent with the observed temperature dependences for chain initiation, propagation, and termination. As seen in Fig. 10, increasing temperature has virtually no effect on  $k_i$ , but increases both  $k_p$  and  $k_t$ . Since  $E_t$  is larger than  $E_p$ , the rate of chain termination increases more rapidly than the rate of chain propagation, with the result that the surface coverage by growing alkyl chains decreases, whereas the coverage by monomeric building units increases. The total coverage by reaction intermediates is

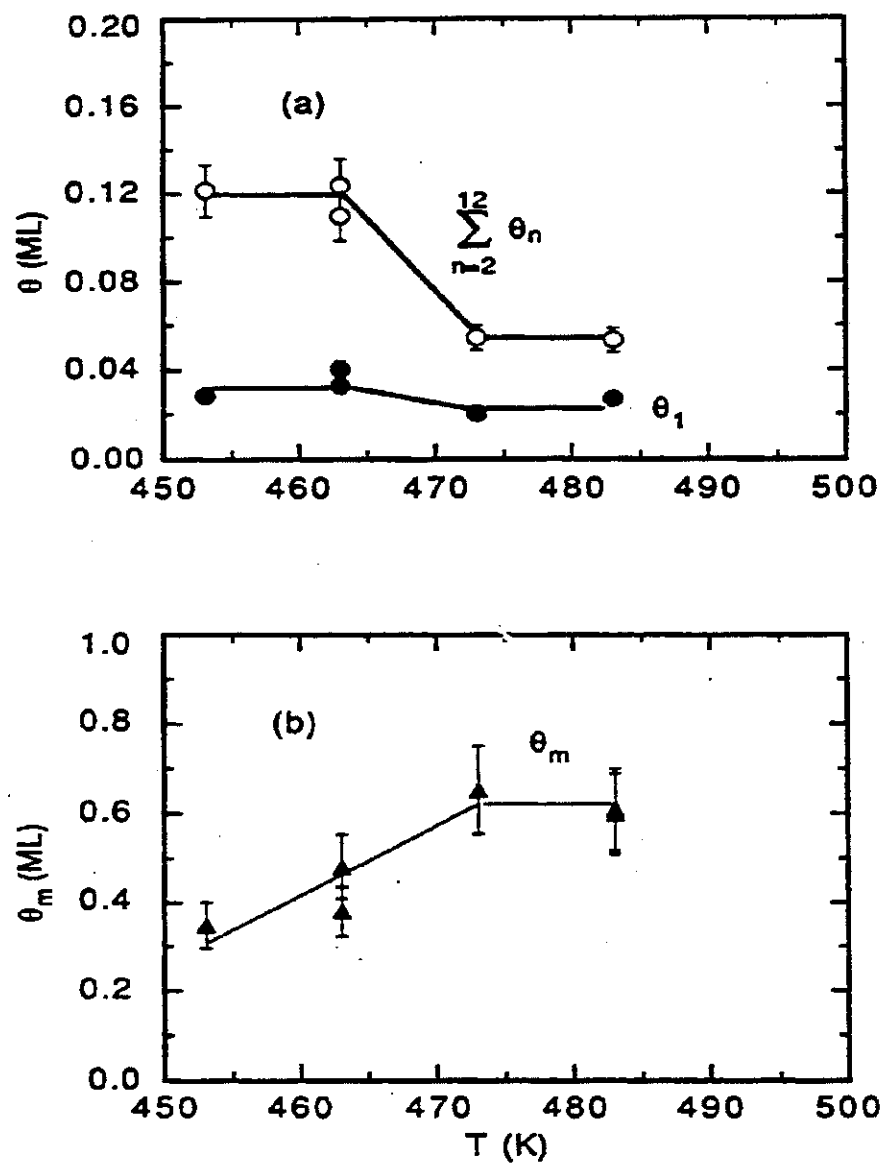


Fig. 11 (a) Coverage by alkyl surface species as a function of temperature; (b) Coverage by monomeric species as a function of temperature;  $D_2/CO = 3$ .

TABLE 5

Coverage by reaction intermediates:  
 $D_2/CO = 3$ , reaction temperature is varied.

T (K)	$\theta_1$ (ML)	$\sum_{n=2}^{12} \theta_n$ (ML)	$\theta_m$ (ML)	Total $\theta_{(n+m)}$ (ML)	$\theta_{CO}$ (ML)
453	0.03	0.12	0.35	0.5	-
463	0.03	0.11	0.38	0.52	0.67
463	0.04	0.12	0.48	0.64	0.67
473	0.02	0.05	0.62	0.69	-
483	0.03	0.05	0.61	0.69	0.65
483	0.03	0.61	0.60	0.68	0.65

seen to be between 0.5 and 0.7 of a monolayer.

To determine whether or not the surface coverages estimated from the model are representative of actual coverages by carbonaceous species, a series of temperature-programmed surface reactions were carried out. Using the techniques described in ref. (27), measurements were made of the CO uptake capacity of the freshly reduced catalyst, the CO uptake of the catalyst after 20 min under reaction conditions, and the total carbon inventory on the catalyst surface, exclusive of CO, after 20 min under reaction conditions. The room-temperature uptake of CO on the freshly reduced catalyst is 1.3 ML. After 20 min of reaction at 463 K and a  $D_2/CO$  ratio of 3, the CO coverage decreases to 0.67 ML and the total amount of carbon exclusive of CO is 1.08 ML. The last of these figures compares very favorably with the value of  $\sum n\theta_n = 1.03$  obtained from the simulation of the transient response experiments. Moreover, the sum of  $\theta_{CO}$  plus  $\sum \theta_n$  for  $n=1-13$  is equal to 1.19-1.31 ML (see Table 5), in good agreement with the initial CO uptake capacity of the catalyst, 1.3 ML. A similar level of agreement is observed when the reaction is carried out at 483 K.

The close correspondence between the predicted and experimentally observed coverages by carbon indicates that the dynamics of the transient response experiments are governed primarily by the  $\alpha$  (carbide) and  $\beta'$  (growing alkyl chains) forms of surface carbon (21). As noted by Krishna and Bell (27), these forms of carbon exhibit time constants that are much shorter than that associated with the build up and consumption of  $\beta''$  carbon, which

contribute to the slow deactivation of Ru.

The observation of a higher surface coverage by monomeric units than by growing chains is qualitatively consistent with the findings of Yokomizo *et al.* (21) for Ru/TiO<sub>2</sub> and Mims *et al.* (16) for Co/Al<sub>2</sub>O<sub>3</sub>. Yokomizo *et al.* (21) estimate the surface coverage by all C<sub>1</sub> species to be 0.25 ML, and the coverage by C<sub>2+</sub> chains to be about 0.10 ML. This compares favorably with the present results which indicate a surface coverage of 0.12 ML by C<sub>2+</sub> species and a coverage of 0.4 by all C<sub>1</sub> species. Since the estimates of surface coverages reported here and by Yokomizo *et al.* (21) are based on completely different methods, the degree of agreement is all the more remarkable.

Figure 12 indicates the effects of D<sub>2</sub> partial pressure on k<sub>i</sub>, k<sub>p</sub>, and k<sub>t</sub>. The value of k<sub>p</sub> is essentially independent of the partial pressure of D<sub>2</sub>, consistent with what would be expected, since chain growth does not involve adsorbed D atoms. By contrast, the value of k<sub>t</sub> rises linearly with increasing D<sub>2</sub> partial pressure. This trend can be explained in the following manner. As defined, k<sub>t</sub> is an apparent rate coefficient representing termination to olefinic and paraffinic products. Expressing k<sub>t</sub> in terms of its component parts gives

$$k_t = k_t^{\bar{}}\theta_v + k_t^{\cdot}\theta_D \quad (13)$$

where  $k_t^{\bar{}}$  and  $k_t^{\cdot}$  are the rate coefficients for termination to olefins and paraffins, respectively, and  $\theta_v$  and  $\theta_D$  are the vacancy and D atoms surface coverages, respectively. The increase in k<sub>t</sub> with D<sub>2</sub> partial pressure can, therefore, be attributed to the increase in  $\theta_D$ .

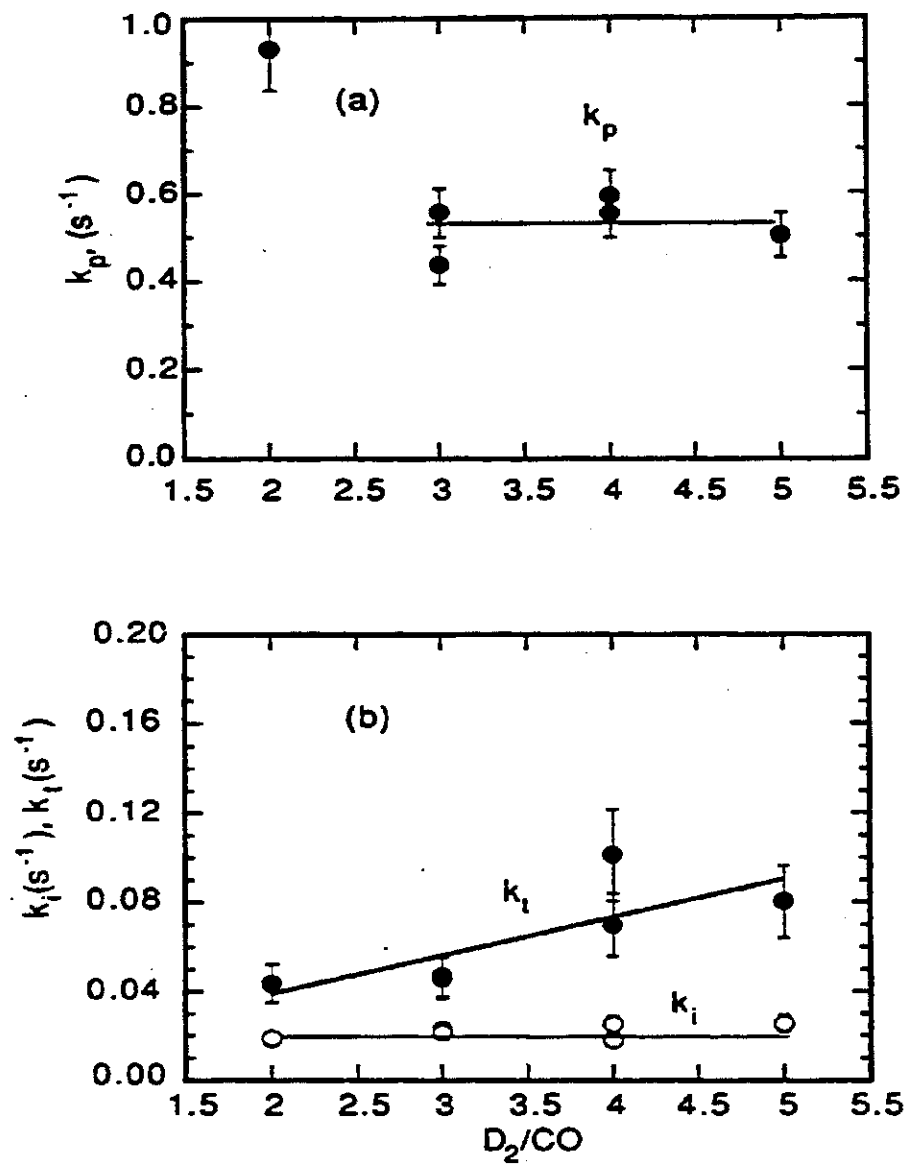


Fig. 12 (a) Propagation rate constant,  $k_p$ , as a function of  $D_2/CO$  ratio; (b) Initiation rate constant,  $k_i$ , and termination rate constant,  $k_t$ , as a function of  $D_2/CO$  ratio

In agreement with this, the product distribution shifts to more paraffinic products as the  $D_2$  partial pressure rises (see Fig. 7e). Equation 13 also helps explain the weak dependence of the olefin to paraffin ratio on temperature, seen in Fig. 7c. Since  $\theta_D$  decreases and  $k_i$  increases with temperature, the product of  $\theta_D$  and  $k_i$  should show a weaker temperature dependence.

The independence of  $k_i$  on  $D_2$  partial pressure is puzzling, since as discussed above, this rate coefficient is, in fact, the product of an intrinsic rate coefficient and  $\theta_D$ . No explanation can be given for why  $k_i$  does not behave in the same manner as  $k_t$ .

The dependence of the surface coverages of carbonaceous species calculated from the model is given in Fig. 13 and Table 6. The coverage by monomeric building units and  $C_1$  chain initiators increases with  $D_2$  partial pressure and approaches a constant value, whereas the surface coverage by  $C_{2-12}$  chains appears to pass through a maximum. The trends in  $\theta_m$  and  $\theta_1$  indicate that with decreasing  $D_2$  partial pressure, the rate of conversion of nascent carbon atoms to  $CH_x$  species is somewhat faster than the consumption of these species to form reaction products. The total coverage by reactive species is seen to increase from 0.4 to 0.8 ML as the  $D_2/CO$  ratio is changed.

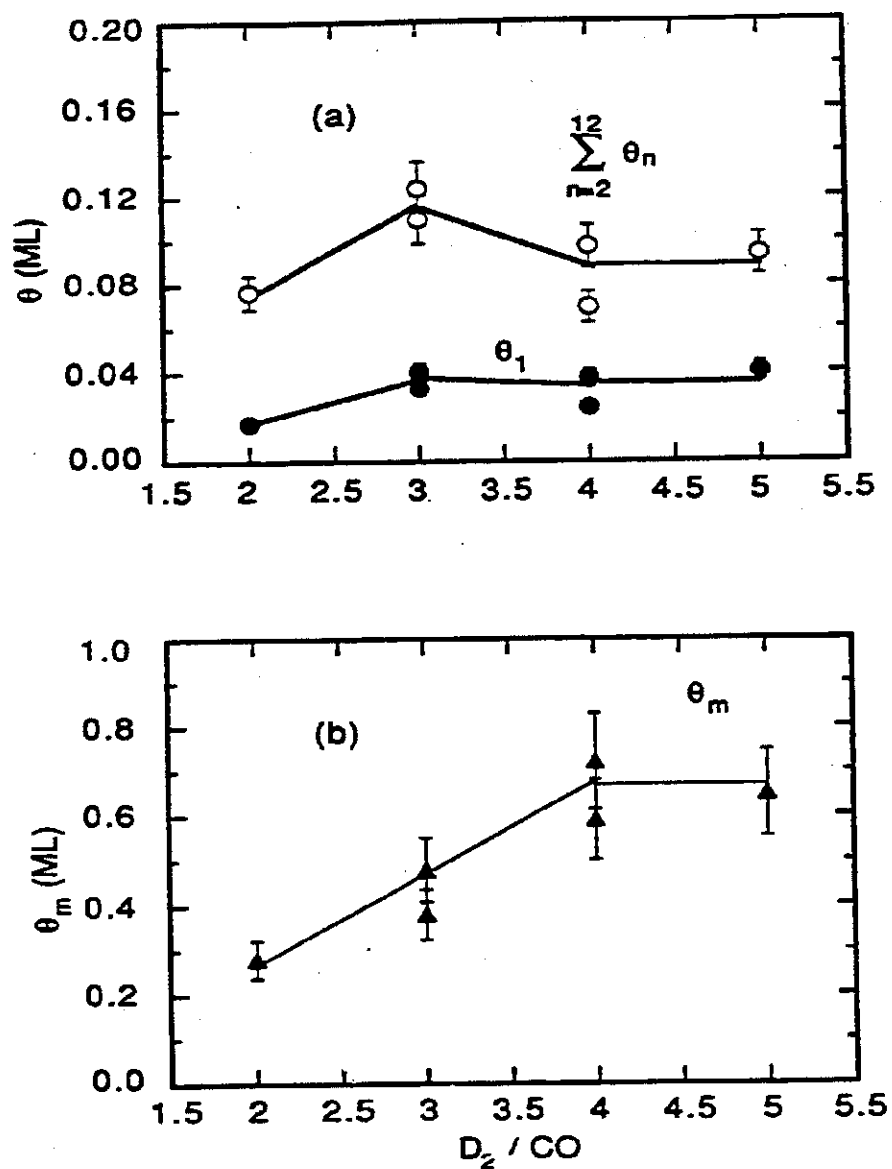


Fig. 13(a) Coverage by alkyl surface species as a function of  $D_2/CO$  ratio; (b) Coverage by monomeric species as a function of  $D_2/CO$  ratio;  $T = 463$  K.

TABLE 6  
Coverage by reaction intermediates:  
D<sub>2</sub>/CO ratio is varied, T= 463 K.

D <sub>2</sub> /CO	θ <sub>1</sub> (ML)	$\sum_{n=2}^{12} \theta_n$ (ML)	θ <sub>m</sub> (ML)	Total θ <sub>(n+m)</sub> (ML)
2	0.03	0.12	0.28	0.43
3	0.03	0.11	0.38	0.52
3	0.04	0.12	0.48	0.64
4	0.02	0.07	0.72	0.81
4	0.04	0.10	0.59	0.73
5	0.04	0.10	0.65	0.79

## CONCLUSIONS

Isotopic tracer methods have been used to determine the dynamics of chain initiation, propagation and termination for Fischer-Tropsch synthesis over Ru/TiO<sub>2</sub>. Values for the rate coefficients  $k_i$ ,  $k_p$  and  $k_t$  were determined by fitting theoretically generated transient response curves to those obtained experimentally. The rate coefficient for chain initiation,  $k_i$ , is independent of both temperature and D<sub>2</sub>/CO ratio. The rate coefficient for chain propagation,  $k_p$ , has an activation energy of 8 kcal/mol, but is independent of the D<sub>2</sub>/CO ratio. The rate coefficient for chain termination,  $k_t$ , has an activation energy of 20 kcal/mol and increases linearly with D<sub>2</sub>/CO ratio. The higher activation energy for chain termination than that for chain propagation explains the observed decrease in probability of chain growth,  $\alpha$ , with increasing temperature.

The surface coverages by various carbonaceous species have also been determined from an analysis of the fitted transient response curves. It is concluded that the dominant species are monomeric building units, which occupy 0.2 to 0.6 ML. Growing alkyl chains, the direct precursors to hydrocarbon products occupy  $\leq 0.2$  ML. Adsorbed CO occupies an additional  $\approx 0.7$  ML. These estimates are found to be in good agreement with independent measurements made by temperature-programmed reaction spectroscopy.

## APPENDIX

The apparent rate constant for propagation,  $k_p\theta_m$ , and the rate constant for termination,  $k_t$ , are calculated from  $\alpha$  and  $\tau$  using the following equations:

$$\alpha = \frac{k_p \theta_m}{k_p \theta_m + k_t} \quad (\text{A1})$$

and

$$\tau = \frac{1}{k_p \theta_m + k_t} \quad (\text{A2})$$

The value of  $\tau$  is determined from a fit of eqn. 12 to the observed curves of  $F_n(t)$ .

The monomer coverage,  $\theta_m$ , is calculated as follows. At steady-state, the rate of CO consumption must equal the rate at which monomeric species are consumed. This equality can be written as:

$$N_{\text{CO}} = \frac{\theta_m}{\tau_m} \quad (\text{A3})$$

Since  $N_{\text{CO}}$  is known from steady-state rate measurements and  $\tau_m$  is known from the fit of eqn. 12 to the observed curves  $F_n(t)$ ,  $\theta_m$  can be evaluated. The value of  $k_p$  can be determined from eqn. A2.

The value of  $k_i$  can be calculated by recognizing that the rate at which carbon atoms are consumed from the  $C_1$  pool is equal to the rate at which carbon atoms enter this pool. This leads to eqn. A4.

$$\frac{\theta_1}{\tau} = k_i \theta_m \quad (\text{A4})$$

Since

$$\frac{\theta_1}{\tau} = \frac{\frac{N_{C_1}}{k_1}}{\frac{1}{k_p \theta_m + k_1}} = \frac{N_{C_1}}{1 - \alpha} \quad (\text{A5})$$

$k_1$  can be calculated from eqns. A4 and A5, using the measured values of  $N_{C_1}$  and  $\alpha$ , and the previously determined value of  $\theta_m$ .

The coverages by alkyl species can be calculated from the hydrocarbon turnover frequencies and the value of  $k_1$ . Since

$$N_{C_n} = k_1 \theta_n \quad (\text{A6})$$

then

$$\sum_{n=1}^{n_1} \theta_n = \frac{1}{k_1} \sum_{n=1}^{n_1} N_{C_n} \quad (\text{A7})$$

#### REFERENCES

1. Anderson, R. B., 'The Fischer-Tropsch Synthesis', Academic Press, New York, 1984.
2. Biloen, P. and Sachtler, W. M. H., *Adv. Catal.* **30**, 165 (1981).
3. Kellner, C. S., and Bell, A. T., *J. Catal.* **70**, 418 (1981).
4. Dry, M. E., *Catal.-Sci. and Tech.* **1**, 150 (1981).
5. Dry, M. E., *Catal. Today* **6**, 183 (1990).
6. Bell, A. T., *Catal. Rev.-Sci. Eng.* **23**, 203 (1981).
7. Winslow, P., and Bell, A. T., *J. Catal.* **86**, 158 (1984).
8. Winslow, P., and Bell, A. T., *J. Catal.* **91**, 142 (19845).
9. Biloen, P., Helle, J. N., and Sachtler, W. M. H., *J. Catal.* **58**, 95

- (1979).
10. Bonzel, H. P., and Krebs, H. J., *Surf. Sci.* **91**, 499 (1980).
  11. Kobori, Y., Yamasaki, H., Naito, S., Onishi, T., and Tamaru, K., *J. Chem. Soc., Far. Trans. i* **78**, 1473 (1982).
  12. Biloen, P., Helle, J. N., van den Berg, F. G. A., and Sachtler, W. M. H., *J. Catal.* **81**, 450 (1983).
  13. Orita, H., Naito, S., and Tamaru, K., *J. Catal.* **90**, 183 (1984).
  14. Zhang, X., and Biloen, P., *J. Catal.* **98**, 468 (1986).
  15. Mims, C. A., and McCandlish, L. E., *J. Am. Chem. Soc.* **107**, 696 (1985).
  16. Mims, C. A., and McCandlish, L. E., *J. Phys. Chem.* **91**, 929 (1987).
  17. Stockwell, D. M., and Bennett, C. O., *J. Catal.* **110**, 354 (1988).
  18. Stockwell, D. M., Bianchi, D., and Bennett, C. O., *J. Catal.* **113**, 13 (1988).
  19. Biloen, P., *J. Molec. Catal.* **21**, 17 (1983).
  20. Bennett, C. O., in "Catalysis under Transient Conditions", eds: A. T. Bell and L. L. Hegedus, ACS Symposium Series **178**, 1 (1982).
  21. Yokomizo, G. H., and Bell, A. T., *J. Catal.* **119**, 467 (1989).
  22. Vannice, M. A., *J. Catal.* **37**, 449 (1975).
  23. Vannice, M. A., and Garten, R. L., *J. Catal.* **56**, 236 (1979).
  24. Vannice, M. A., and Sudhakar, C., *J. Phys. Chem.* **88**, 2429 (1984).
  25. Reuel, R. C., and Bartholomew, C. H., *J. Catal.* **85**, 78 (1984).
  26. Rieck, J. S., and Bell, A. T., *J. Catal.* **99**, 262 (1986).
  27. Krishna, K. R. and Bell, A. T., *J. Catal.* **130**, 597 (1991).
  28. Sano, M., Yotsui, Y., Abe, H., and Sasaki, S., *J. Biomed. Mass Spec.* **3**, 1 (1976).
  29. Matthews, D. E., and Hayes, J. M., *Analyt. Chem.* **50**, 1465 (1978).

30. Jordan, D. S., and Bell, A. T., *J. Phys. Chem.* **90**, 4797 (1986).
31. Jenson, V. G., and Jeffreys, G. V., "Mathematical Methods in Chemical Engineering", Second Edition, Academic Press, 1977.
32. Dictor, R. A., and Bell, A. T., *Appl. Catal.* **20**, 145 (1986).
33. Schulz, H., *C<sub>1</sub> Molec. Chem.* **1**, 231 (1985).
34. Froment, G. F., and Hosten, L. H., *Catal.-Sci. and Tech.* **2**, 97 (1981).
35. Box, G. E. P., Hunter, W. G., and Hunter, J. S., "Statistics for Experimenters", John Wiley and Sons, 1978.
36. Shustorovich, E. and Bell, A. T., *Surf. Sci.* **248**, 359 (1991).